Communs geol. Surv. Namibia, ***10*** *(1995), 5-20*

Pressure-temperature evolution of a low-pressure amphibolite facies terrane in central Bushmanland (Namaqua Mobile Belt; South Africa)

A.P. Willner
Institut für Mineralogie, Ruhr-Universität, -.44780 Bochum, Germany

The Bushmanland subprovince of the Namaqua Mobile Belt is characterised by HT/LP metamorphism around 1100 Ma over a 200-300 km-wide zone with continuous N-S zoning from amphibolite to granulite facies terranes. The thermal peak of metamorphism is preceded by convergent tectonics with thrusting of previously thinned crust and major intrusions of synkinematic granitoids. While the granulite facies terrane shows an anticlockwise PT-path and isobaric cooling at a level corresponding to 5 kbar (Waters, 1990), the adjacent amphibolite facies zone is characterised by a clockwise PT-path. The PT-evolution may be generalised as follows: Pseudomorphs after andalusite in topazites indicate that the prograde path crossed its stability field. A further prograde relic is fibrolite that to some extent grew parallel to the stretching lineation of the major SW-directed thrust event. Fibrolitisation of feldspars, garnets, micas and spinel in contact with fibrolite indicate cation solution. It can be shown that this is an effect of prograde increase in temperature and pressure during continuous hydrous fluid flow. Relic inclusion phases in garnets of pelites and peraluminous rocks point to an equilibrium stage at 600°C/4 kbar after crustal stacking. Isobaric heating follows until the thermal maximum is reached at 680°C/4 kbar accompanied by anatexis. This is in contrast to the adjacent granulite terrane, where isobaric cooling follows the pressure peak. The early retrograde PT-path involves penetrative growth of coarse white mica and decompression of 1.5 kbar during cooling to 580°C. A late retrograde growth of low grade phases is caused by a penetrative infiltration of external fluids at 1.5 kbar/300-400°C. It is suggested that crustal stacking occurred in a warm thinned crust with basic magmatic underplating before and during convergence. The contrasting direction of the PT-paths of the amphibolite and the adjacent granulite terrane after reaching of the pressure maximum is interpreted as thermal relaxation towards a joint geotherm of about 45-50°C/km. This was the result of conductive heat transport after stacking of a crustal slice with an initially relatively lower geotherm over a slice with an initially relatively higher one. The convergence and related PT-evolution under elevated geotherms must have occurred in the inner part of a wide magmatic arc of a convergent Andean-type continental margin.

Introduction

With recent advances in understanding of high grade metamorphic terranes and the development of tectonothermal models, an important group of large low pressure granulitic areas especially in Proterozoic orogens became well known. This group is characterised by low to medium pressures, heating during increase of pressure by crustal stacking, and early retrograde isobaric cooling (IBC-type: Harley, 1989; Waters, 1990) defining an anticlockwise PT path. Magmatic accretion and advection is generally involved in models for such terranes. For a further crustal-scale interpretation, especially the study of related crustal slices of lower temperature and higher crustal levels is important, which may be directly related to such terranes. An ideal crustal section with continuous prograde transition from amphibolite facies areas to well studied granulites of the IBC-type is found in the Namaqua Mobile Belt of South Africa (Waters, 1986; 1990, Fig. 1). The scope of this paper is to recognise successive equilibrium stages and to provide respective pressure-temperature data. On this basis it is intended to model a PT-path for such a LP/HT amphibolite terrane structurally overlying IBC-granulites and to correlate the crustal dynamic evolution of both areas.

Central Bushmanland (Northern Cape Province) is part of the Namaqua-Natal Mobile Belt which surrounds the Archaean Kaapvaal craton in the SE and W (Fig. 1). It consists of 2000-1000 Ma old supracrustal volcanosedimentary sequences and predominantly synkinematic granitoid intrusions. Metamorphic zoning comprises greenschist up to granulite facies areas with high grade terranes dominating. The belt is essentially a HT/LP province with pressures not exceeding 6 kbar. The major crustal dynamic evolution was during the Namaqua Orogeny around 1250-1000 Ma (equivalent to the Kibaran event). Crustal growth probably occurred by multiple lateral accretion of crust during formation of continental magmatic arcs along a Proterozoic convergent continental margin over a long period (Hartnady *et al.*, 1985).

Several subprovinces of the Namaqua Mobile Belt are separated by regional ductile-thrust and strike-slip shear zones. Within the Bushmanland subprovince a simple continuous transition is found over more than 200 km from amphibolite facies areas especially in central Bushmanland to wide granulite facies areas toward the S in Namaqualand. No temperature or pressure jumps were recognised and isograds are parallel to the E-W strike of late open megafolds (Waters, 1986, 1990). Deformational history within the entire Bushmanland subprovince is regarded as uniform and with dominating structures of horizontal tectonics related to crustal stacking during the prograde PT-path (Hartnady *et al.*, 1985; Joubert, 1986; Strydom and Visser, 1986; Van der Merwe and Botha, 1989; Waters, 1990).

Geological setting

Central Bushmanland (Fig. 2) is separated from the Richtersveld province towards the north by the Groothoek thrust (Blignault *et al.*, 1983; Van der Merwe and Botha, 1989), where rocks with older deformational imprints (2000 Ma Orange River Orogen) are thrust over the supracrustal Bushmanland Supergroup with

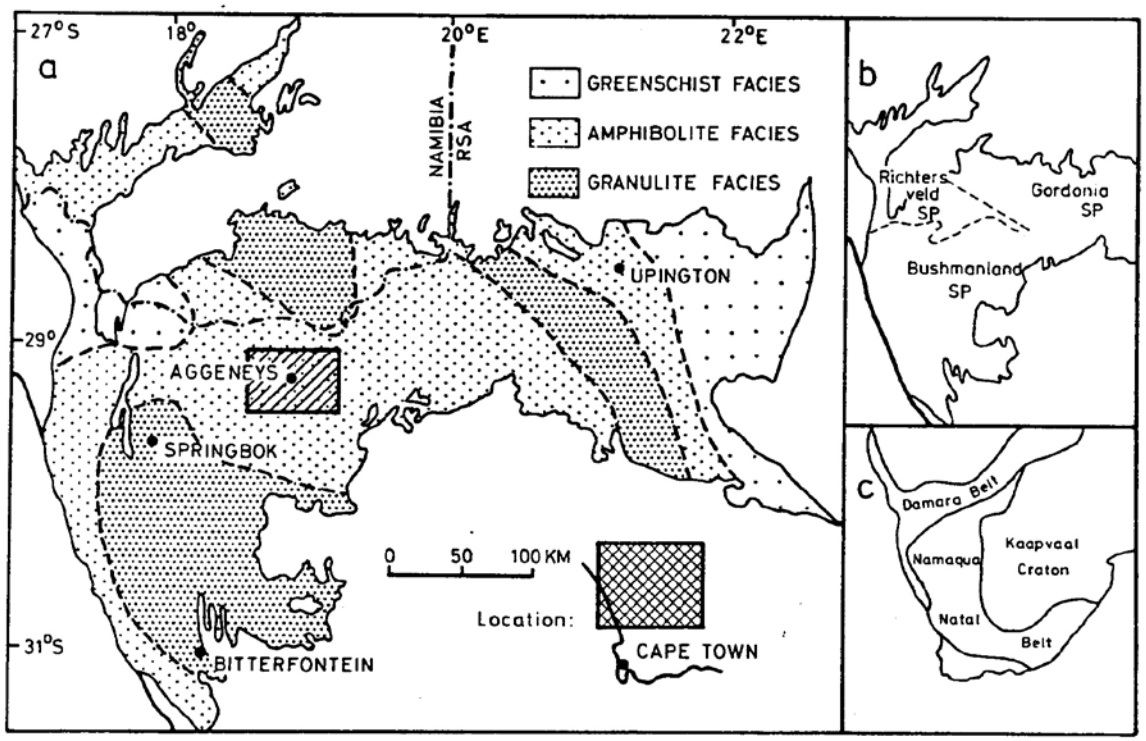

Figure 1: Location of central Bushmanland and distribution of metamorphic facies according to Joubert (1986); **b** - Simplified subdivision of the Namaqua Mobile Belt according to Hartnady *et al.* (1985); **c** - geotectonical subdivision of southern Africa simplified after Hartnady *et al.* (1985).

a depositional age probably around 1650 Ma (Reid *et al.*, 1987). The volcanosedimentary supracrustal sequence overlies thick stratiform orthogneisses which are regarded as metarhyolites (Moore 1986). The metasediments are mainly pelites and thick quartzites with intercalations of rare peraluminous rocks (sillimanite-corundum rocks, topazites) at the base related to laterally occurring tourmalinites, gahnite-quartzites and calcsilicate rocks. In the upper part of the sequence stratiform massive sulfides (Aggeneys/Gamsberg deposits) with lateral iron formations and orthoamphibolites are intercalated. The depositional environment is interpreted as an intracontinental rift regime characterised by bimodal volcanism, shallow marine clastic and exhalative sedimentation (Moore, 1986; Colliston *et al.*, 1986).

The subhorizontal layering and main foliation in central Bushmanland is interpreted by all structural workers as an effect of large-scale crustal stacking of thin sedimentary units with ductile thrust zones subparallel to former bedding including sheath folds on all scales (D_2 after Joubert, 1974). The Groothoek thrust is regarded as a major D_2 mid-crustal thrust zone marking a main terrane boundary. Ductile amphibolite facies conditions prevailed during thrusting. Progressive increase in homogeneous simple shear is observed from N to S as well as prograde medium to high grade metamorphism in the roof of the thrust sequence (Van der Merwe and Botha, 1989). Megastructures within Bushmanland represent duplex structures related to this thrust event (Blignault *et al.*, 1983; Watkeys, 1986, 1988; Van Aswegen *et al.*, 1987; Colliston *et al.*, 1991). The pronounced D_2-stretching lineation is NE-SW with a consistent transport direction towards the SW. Large synkinematic granite intrusions of sheet -like extent are bound to large D_2-thrust zones (Aroams gneiss and augen gneiss; Duncan *et al.*, 1985). The Aroams gneiss has a concordant U/Pb age of 1100 Ma (Armstrong *et al.*, 1988). The entire stack was deformed to open megafolds, which are probably related to regional strike-slip movements (D_3 and D_4 after Joubert, 1974; Watkeys, 1986). The dominant deformation events (D_1/D_2) occurred prior to the thermal peak of metamorphism.

Method

All mineral analyses were made with a CAMECA microprobe (Camebax) at the Institut für Mineralogie/ Ruhr-Universität Bochum/Germany. Operating conditions were 15 kV acceleration voltage, 14 nA beam current and 20 s measuring time using a slightly defocused beam to minimize alkali loss. Natural and synthetic minerals were used as standards. In Table 1 representative analyses are given. A complete list may be given by the author upon request or is provided in Willner (1993). The mode of calculation of structural formula of the minerals is also given in Table. 1. Mineral abbreviations are according to Kretz (1983).

	White Mica		Biotite			
	SA 136		SA 75		SA 136	
	I*	II*	I**	II**	II**	III
SiO_2	46.28	48.31	33.52	33.15	34.48	34.29
TiO_2	1.07	0.08	1.30	1.65	2.75	3.0
Al_2O_3	36.01	35.49	16.93	18.90	19.84	19.54
Cr_2O_3	0.03	0.04	0:01	0.02	0.04	0.00
FeO	1.20	1.11	24.40	24.74	18.74	18.98
MnO	0.03	0.00	0.05	0.07	0.32	0.26
MgO	0.50	0.62	8.45	5.80	8.92	8.96
CaO	0.00	0.00	0.00	0.00	0.03	0.03
BaO	0.09	0.12	0.02	0.04	0.02	0.00
Na_2O	0.51	0.34	0.07	0.08	0.09	0.14
K_2O	10.55	10.36	9.68	9.52	9.72	9.59
F	0.03	0.03	1.00	0.51	0.12	0.17
Cl	0.00	0.03	0.08	0.11	0.03	0.03
H_2O	4.54	4.57	3.27	3.48	3.85	3.82
Sum[1)]	100.84	101.07	98.34	97.83	98.97	98.80
	Ions based on 22 oxygens					
Si	6.101	6.311	5.335	5.294	5.275	5.259
Al^{IV}	1.899	1.689	2.665	2.706	2.725	2.741
Al^{VI}	3.695	3.776	0.510	0.850	0.851	0.791
Ti	0.106	0.008	0.156	0.198	0.317	0.351
Cr	0.003	0.004	0.007	0.002	0.005	0.000
Fe	0.132	0.121	3.247	3.304	2.397	2.434
Mn	0.003	0.000	0.007	0.009	0.042	0.033
Mg	0.099	0.120	2.004	1.380	2.033	2.054
Sum	4.038	4.029	5.926	5.744	5.645	5.663
Ca	0.000	0.001	0.001	0.000	0.005	0.005
Ba	0.005	0.006	0.002	0.003	0.001	0.000
Na	0.131	0.087	0.022	0.025	0.027	0.041
K	1.774	1.727	1.965	1.938	1.896	1.876
Sum	1.910	1.821	1.989	1.966	1.929	1.922
F	0.011	0.012	0.504	0.259	0.059	0.085
Cl	0.000	0.005	0.022	0.030	0.008	0.009
OH	3.989	3.983	3.473	3.711	3.933	3.906
n	5	1	1	5	5	1

	Garnet				Plagioclase		K-fsp
	SA 136		Sa 75				
	core	rim	core	rim			
SiO_2	36.34	36.62	36.24	36.25	SiO_2	62.24	64.61
TiO_2	0.01	0.04	0.00	0.01	Al_2O_3	24.20	18.81
Al_2O_3	20.59	21.39	20.67	20.57	Fe_2O_3	0.04	0.00
Cr_2O_3	0.02	0.01	0.00	0.00	BaO	0.06	0.32
Fe_2O_3	0.98	0.32	1.18	1.01	CaO	5.18	0.00
FeO	28.46	29.36	37.45	36.88	Na_2O	8.63	1.33
MnO	8.88	9.40	1.51	3.79	K_2O	0.19	14.77
MgO	3.30	2.89	2.07	1.10	Sum	100.53	99.85

Table 1: Representative mineral analyses of two pelite samples (continued on page 8).

CaO	1.12	1.03	1.32	1.13	Ions	based on 4	Oxygens
Sum	99.76	100.85	100.44	100.88	Si	2.746	2.981
	Ions based on 24 oxygens				Al	1.258	1.023
Si	5.921	5.895	5.895	5.919	Fe^{3+}	0.001	0.000
Al^{IV}	0.079	0.105	0.105	0.081	Sum	4.005	4.004
Al^{VI}	3.876	3.955	3.858	3.877	Ca	0.245	0.000
Cr	0.003	0.002	0.000	0.000	Na	0.738	0.119
Fe^{3+}	0.120	0.039	0.142	0.122	K	0.011	0.869
Ti	0.001	0.005	0.000	0.001	Sum	0.995	0.994
Sum	4.000	4.000	4.000	4.000			
Mg	0.802	0.693	0.502	0.268			
Fe^{2+}	3.878	3.913	5.113	5.051			
Mn	1.226	1.282	0.208	0.524			
Ca	0.195	0.178	0.230	0.198			
Sum	6.101	6.067	6.053	6.041			

* White Mica I - Matrix white mica
White Mica II - Late retrograde white mica
** Biotite I - Inclusion in garnet
Biotite II - Matrix biotite
Biotite III - Biotite in contact with garnet r

n Number of analyses
1) Sum corrected for halogens

Table 1: Representative mineral analyses from two pelite samples (continuation).

Petrography

Pelites

Qualitative and quantitative modal composition of pelites in all lithostratigraphical units of central Bushmanland is rather uniform: Quartz-sillimanite-muscovite-biotite ± garnet ± K-feldspar ± plagioclase. Accessories are ilmenite, magnetite, green spinel, tourmaline, zircon and monazite. The dominant fabric includes secondary post-kinematic recrystallisation of coarse quartz and feldspars with inclusions of biotite, muscovite, garnet and sillimanite (Fig. 3) as well as post-kinematic mimetic growth of coarse micas parallel to a relic main foliation. This represents long static heating at high temperatures.

Conspicuous is a dominantly high content of sillimanite (5-20 vol%) occurring as fibrolite nodules or layers, more rarely as nests of prismatic sillimanite. Banding due to the fibrolite enrichments alternating with biotite-rich laminae, parallels the main foliation. Fibrolite may form unorientated aggregates, but may also be strongly orientated parallel to the regional stretching lineation (SW-NE) as the only relict phase. Orientated fibrolite is mainly preserved within coarse quartz (Fig. 4). On the other hand, coarse prismatic sillimanite is always unorientated and recrystallises from fibrolite nodes (Fig. 5). Hence fibrolite is an older variety than prismatic sillimanite formed under static peak conditions.

Locally biotite or garnet may be decomposed to fibrolite in various degrees, finally decomposing entirely to fibrolite (Fig. 6), while they are otherwise Stable phases in the matrix nearby. Some horizons in pelites and stratiform orthogneisses are even characterised by oval fibrolite nodules of mm to cm scale (Fig. 4). They are partly concentrated in zones of locally enhanced strain and orientated by prograde D_2-thrusting (Watkeys, 1986; Odling, 1988). These nodules prove local corrosion of feldspars and micas by ionic reactions.

Abundant coexistence of K-feldspar and sillimanite indicates that the muscovite-quartz out-isograd was overstepped. Following fabrics indicate early retrograde muscovite growth mainly due to fluid-rock interaction:

- muscovite grows across fibrolite nodules (Fig. 4, 7) starting at sillimanite-quartz grain boundaries
- muscovite grows epitactically on grain boundaries of biotite or magnetite
- quartz-muscovite symplectites grow at expense of K-feldspar, but also in rocks lacking K-feldspar, e.g. at expense of fibrolite (Fig. 7).
- muscovite always grows post-kinematically in F_2 fold hinges

Yet, within intercalated pure quartzites, muscovite

occurs as inclusions within coarse quartz. This apparently older generation of muscovite is obviously bound to the quartzitic intercalations.

Two stages of garnet growth may be observed. Cores rich in inclusions of fine-grained quartz, biotite and fibrolite that may be orientated, represent an early generation of garnet growth across a fine-grained matrix. A second generation is generally represented by rims or separate grains with few inclusions, in some cases as skeletal grains grown in a coarse matrix. Some garnets form as rims around biotite. Garnet grain boundaries are rounded, partly rimmed by biotite or fibrolite.

Abundant peak metamorphic phenomena are observed as unfoliated anatectic neosomes composed of both feldspar and quartz in pelites and stratiform orthogneisses as well as mobilised pegmatoids.

Late sericite grows at the expense of quartz, plagioclase and sillimanite. Chlorite also is an abundant retrograde phase.

Peraluminous rocks

Early descriptions of abundant rocks of peraluminous composition that were mined in the past for sillimanite are given by Frick and Coetzee (1974) and Moore (1977). These rocks form lenticular bodies of several metres up to 90 m in thickness containing primarily sillimanite-, sillimanite-corundum rocks and sillimanite-quartz-schists. Two main parageneses are:

sillimanite-muscovite-rutile ± topaz ± biotite *and*
sillimanite-corundum-biotite-rutile ± fluorite ± muscovite.

Accessories are monazite, zircon, anorthite, tourmaline, green spinel, pyrite and ilmenite. All quartz-free peraluminous rocks lack any orientation in contrast to the sillimanite-quartz-schists. Both fibrolitic and prismatic sillimanite generations occur (Fig. 5), which are decomposed partly by retrograde pyrophyllite, diaspore and kaolinite. Prograde decomposition of biotite or green spinel in contact with fibrolite and retrograde growth of muscovite at expense of fibrolite are abundant.

Local intercalations are topazites with topaz as the main constituent including prismatic sillimanite needles, rutile and minor corundum, biotite or muscovite. Important are coarse pseudomorphs of topaz, after a prismatic phase with rhombic cross sections, which is regarded to be andalusite (Fig. 8; Schreyer, 1987; Willner, 1993). Also anorthite, tourmaline, ilmenite, rutile, green spinel, dumortierite, pyrite and apatite may be rock forming minerals in local stratiform peraluminous rock types of exhalative origin, which may also occur laterally in quartz-rich horizons. Rounded inclusions of staurolite, corundum and sulphide within spinel from spinel-sillimanite rocks, which are not found in mutual contact, are regarded as relic prograde phases. Fine-grained round inclusions of spinel or tourmaline in coarse quartz grains can be regarded as relics of a lower temperature fabric. Similar features are also found in calcsilicate rocks and iron formations in the area. Typical for all these rock types is a strain-free polygonal fabric with bimodal grain size distribution (0.05-0.1 mm and 0.5-1 mm)

Calcsilicate rocks

Calcsilicate rocks occur as small lenses in different stratigraphic positions of the Bushmanland Supergroup. Observed parageneses are:
garnet-quartz-anorthite-sphene-clinopyroxene
tremolite-clinopyroxene-quartz-anorthite-sphene- fluorite

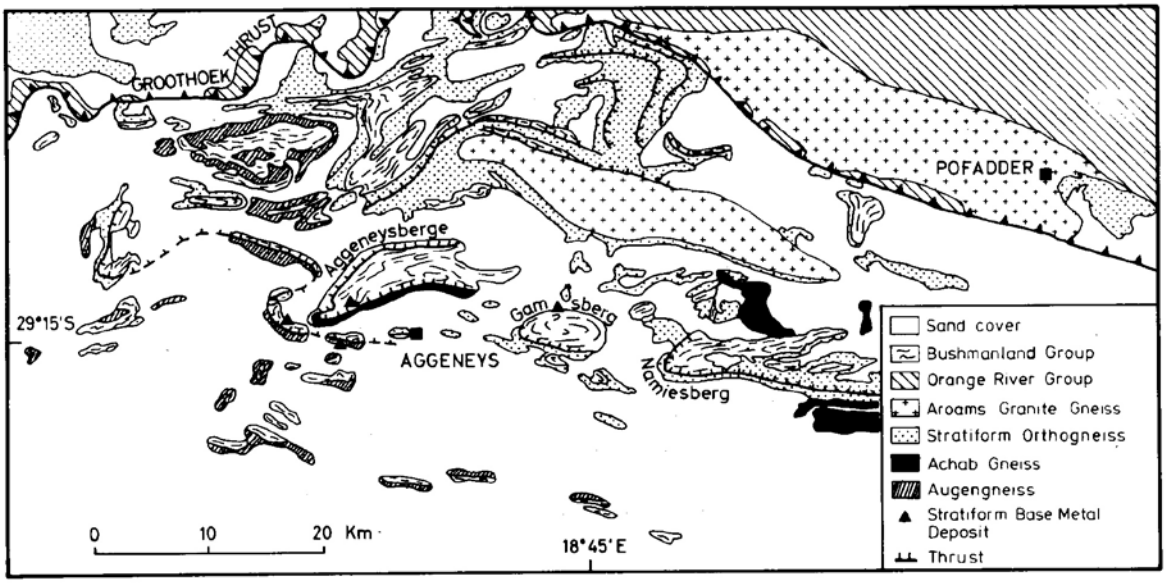

Figure 2: Simplified geological map of central Bushmanland after Duncan *et al.* (1985).

Figure 3: Garnet with inclusions of biotite and fibrolite orientated parallel to main foliation in pelite. Width of photo 4.5 mm; plane-polarised light.

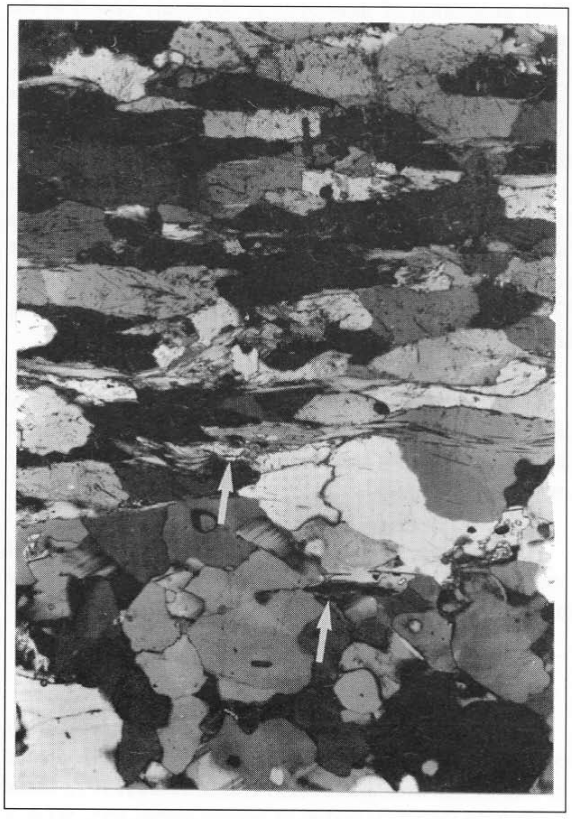

Figure 4: Transition of a fibrolite-quartz-nodule with orientated fibrolite to an unorientated quartz-feldspar-matrix with retrograde muscovite (arrows) in orthogneiss. Width of photo 5.5 mm; crossed polars.

hornblende-clinopyroxene-quartz-anorthite-sphene
hornblende-garnet-quartz-sphene ± biotite ± clinopyroxene + plagioclase.

Polygonal aggregates of plagioclase and amphiboles are typical, while grossular-rich garnet and clinopyroxene occur as xenoblasts rich in inclusions (anorthite, calcite, epidote, sphene).

Constraints for the PT-path

Prograde PT-evolution

In spite of a long-lasting high temperature imprint, abundant information on the prograde PT-path may be derived from relict inclusion phases and pseudomorphs in pelites and peraluminous rocks, and from the interpretation of ion reaction phenomena involving phases in contact with fibrolite.

Evidence of an earliest equilibration are the pseudomorphs of topaz after andalusite (Fig. 8; Schreyer, 1987; Willner, 1993). Such replacement does not necessarily involve external addition of fluorine, but is due to breakdown of the F-rich aluminosilicate zunyite $[Al_{13}Si_5O_{20}F_2(OH,F)_{16}Cl]$ and andalusite to form topaz and corundum (Willner, 1993). The pseudomorphs indicate that at a low temperature stage, the PT-path should have passed the andalusite stability field.

Relict staurolite and corundum inclusions in spinel of spinel-sillimanite rocks that are not in mutual contact are related to the continuous breakdown reaction, staurolite + corundum = spinel + sillimanite, which occurs at low pressures (at higher pressures, spinel and sillimanite are the breakdown products of garnet and corundum). In Fig. 9 the reaction curve for the actual staurolite and spinel compositions was calculated by Willner (1993). Apparently it is lower than the peak temperatures reached in central Bushmanland.

Within the metapelitic gneisses, inclusions of biotite in garnets (Fig. 3) consistently show a lower X_{Fe} [Fe/(Fe+Mg)] than matrix biotites (7 samples) indicating relict compositions of an earlier equilibration stage (Table 1). Detailed analyses of garnet composition around those inclusions show no differences at the immediate contact suggesting restricted exchange between both phases after the inclusion event. In Fig. 8, an X_{Fe} isopleth of a biotite inclusion is drawn (X_{Fe}=0.62) which occurs within a Mn-free paragenesis, garnet-sillimanite-quartz-muscovite. Fibrolite inclusions in some garnets (Fig. 3) suggest that this paragenesis was Stable during early biotite equilibration. The slope of the isopleth indicates strong pressure dependence. It also

indicates that the prograde PT-path came from lower temperatures and/or slightly higher pressures. At lower temperatures and pressures the alternative parageneses staurolite-sillimanite-quartz-muscovite or cordierite-sillimanite-quartz-muscoyite could have occurred within the same whole rock chemistry (Fig. 9). The isopleih for the Mn-free inclusion biotite within such parageneses would give a lower T and P limit. On the other hand the calculated staurolite+corundum breakdown curve from compositions of the protected relics in spinel-sillimanite rocks give a rough temperature for the prograde equilibration. An equilibration stage at about 600°C at 4 kbar can be derived suggesting near isobaric heating prior to peak temperature conditions. Numerous inclusions of medium temperature relict phases prove the existence of an earlier prograde equilibration stage in other rock types, e.g. epidote in garnet of calcsilicate rocks.

A very pronounced prograde feature is cation solution of phases such as biotite, feldspars, garnet or spinel occurring in close contact with fibrolite (Fig. 6). Textural evidence shows that fibrolite is an early sillimanite variety grown parallel to the stretching lineation of the prograde thrust event. It is the only preserved orientated phase, which however, may locally recrystallise to coarse prismatic sillimanite that is never orientated. Formation of the abundant fibrolite nodes and fibrolite-quartz nodules and observable replacement of biotite or garnet may be due to the following reactions:

2 biotite + 14 H^+ = 2 K^+ + 6 $(Fe,Mg)^{2+}$ + sillimanite + 5 quartz + 9 H_2O

(Fe,Zn)spinel + $SiO_{2(aq)}$ + 2 H^+ = $(Fe,Zn)^{2+}$ + sillimanite + H_2O

(Fe,Mn)garnet + 6 H^+ = sillimanite + 3 $(Fe,Mn)^{2+}$ + 2 quartz + 3 H_2O

2 K-feldspar + 2 H^+ = 2K+ + sillimanite + 5 quartz + H_2O

2 albite + 2 H^+ = 2 Na^+ + sillimanite + 5 quartz + H_2O

anorthite + 2 H^+ = Ca^{2+} + sillimanite + quartz + H_2O

2 muscovite + 2 H^+ = 2 K^+ + 3 sillimanite + 3 quartz + 3 H_2O

All these reactions may be modelled with the GeO-calc-software of Brown *et al.* (1988) for compositions and PT-conditions relevant for central Bushmanland (Fig. 10, 11). It can be proved that all above reactions have a positive slope in diagrams with cation/proton-activity ratios plotted against pressure or temperature (except the muscovite-sillimanite reaction). This means that with increasing pressure and temperature the cation-proton activity ratio of the fluid phase increases and hence the amount of fibrolite during continuous fluid flow. This effect, however, does not explain first nucleation of fibrolite. An alternative interpretation of fibrolitisation by externally derived acid solutions seems improbable. HCI should have been the predominant

Figure 5: Prismatic sillimanite grows across fibrolite in a sillimanite-corundum rock. Width of photo 3.7 mm; crossed polars.

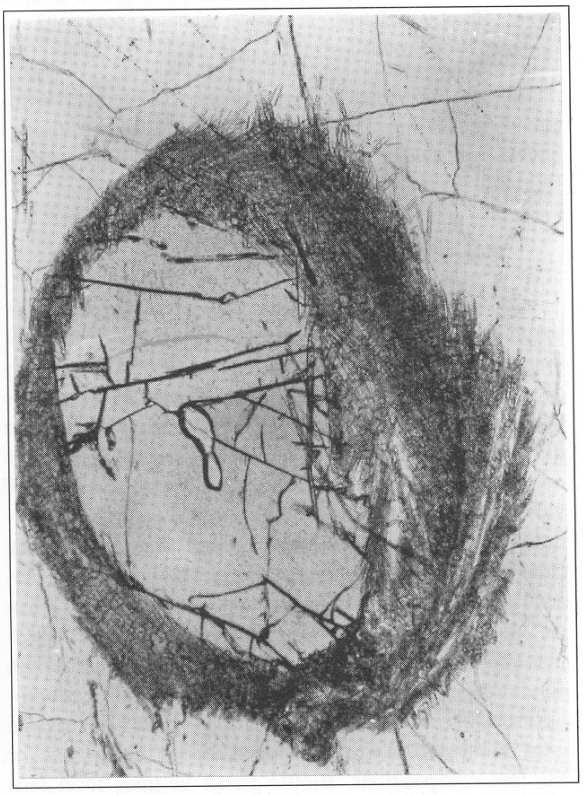

Figure 6: Fibrolitised garnet in pelite. Width of photo 2.3 mm; plane-polarised light.

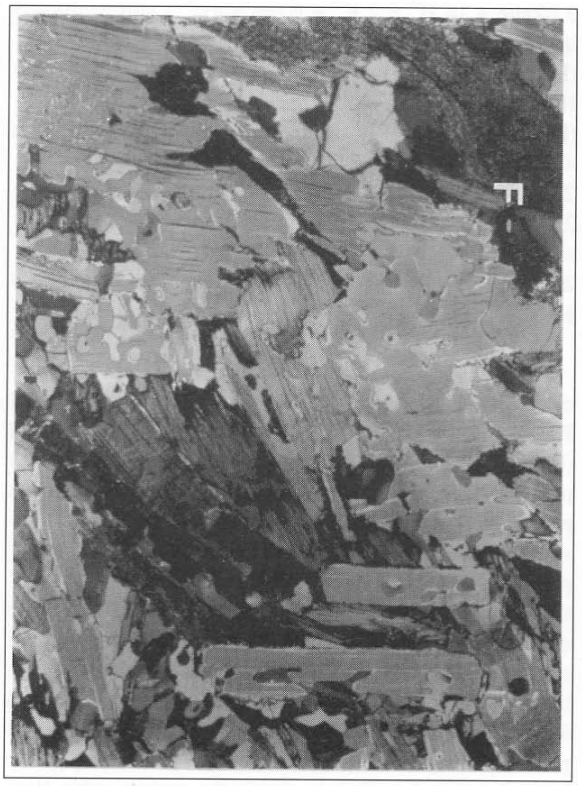

Figure 7: Muscovite-quartz symplectites partly grown across a fibrolite nodule (F) in a pelite. Width of photo is 4.2 cm. Crossed polars.

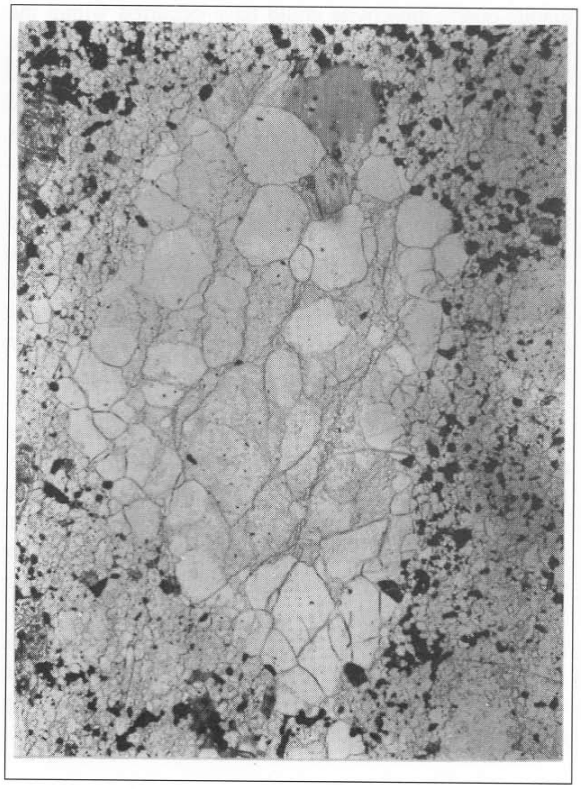

Figure 8: Pseudomorph of topaz after andalusite with rutile bound to the fine-grained matrix in topazite. Width of photo 4.2 mm; plane-polarised light.

pH-controlling fluid species. But this species must have been distributed uniformly within the metamorphic fluid phase, because Cl-activity gradients detectable by systematically measuring mica compositions were entirely homogenised over central Bushmanland already by low external fluid influx (Willner, 1993).

Peak PT data: Thermometry

Garnet-bearing pelites were preferred for geothermobarometry. However, elements apart from the KFMASH-system such as variable Mn in garnets and Ti and F in biotites as well as considerable phase inhomogeneities have to be taken into account. Two types of garnet zoning can be distinguished within the pelites (Fig. 12). Type A shows a marked difference between an unzoned core and a rim of variable size with a marked increase in Mn and the Fe/Mg-ratio. Type B by contrast shows more continuous zoning from core to rim. Coexisting garnet and biotite in paragenesis with sillimanite, muscovite and quartz may be plotted in an enlarged AFM-projection onto the MnO-MgO-FeO-plane (Fig. 13; Spear, 1988). During uniform equilibrium conditions under given pressure and temperature, the compositions of garnets and biotite with variable Mn contents must be situated on a line that meets the Mg-Fe baseline for Mn-free compositions. Biotite-garnet tie-lines form fans (Fig. 13). With increasing Mn contents X_{Mg} in both phases increases considerably. However, within the Bushmanland pelites two groups of matrix biotite-garnet core pairs may be distinguished whose tie-lines cross: Those garnets with type A zoning have garnet cores with a Mn- free composition of $Alm_{90}Pyr_{10}$, those of type B, $Alm_{97}Pyr_{3}$. Projections of the garnet rim compositions and biotites in close contact to the rims show less differences between both groups. This shows that type A garnets still show peak temperature compositions while type B cores are strongly overprinted by retrograde diffusion showing less significant differences between cores and rims. Temperatures were calculated using the Fe/Mg exchange thermometer between biotite and garnet. The calibration of Ganguly and Saxena was applied as well as the thermodynamic data set of Berman (1988) using ideal activity models as well as those of Berman (1990) for garnet and McMullin *et al.* (1991) for biotites with a correction for fluorine as proposed by Perchuk and Aranovich (1984).

The following results were obtained:

Only garnet-core matrix biotite pairs of type A show highest temperatures similar for all methods applied: 690 ± 10°C (4 samples).

Temperatures of garnet rims and biotites in immediate contact are in the range of 500-630°C (7 samples) that is the closing temperature range where diffusion rates exponentially decrease.

Intermediate temperatures in type B garnet cores

indicate a strong retrograde diffusion overprint within these cores.

Independently three calc silicate rock samples with garnet-clinopyroxene pairs yielded similar maximum temperatures of 680-700°C using the Fe-Mg-exchange thermometer as calibrated by Ellis and Green (1979). Zoning was not detected in those garnets, suggesting missing retrograde re-equilibration.

Peak PT-data: Barometry and hygrometry

Only those four selected samples with preserved type A garnet cores in pelites were taken for barometry. Four pressure dependent multivariant reactions were calculated.

(1) $Pyrope_{Grt}$ + $muscovite_{Ms}$ = $phlogopite_{Bi}$ + 2 sillimanite + quartz
(2) $Grossular_{Grt}$ + $muscovite_{Ms}$ + $pyrope_{Grt}$ = 3 $anorthite_{Pl}$ + $phlogopite_{Bi}$
(3) $Almandine_{Grt}$ + $muscovite_{Ms}$ = $annite_{Bi}$ + 2 sillimanite + quartz
(4) $Grossular_{Grt}$ + 2 sillimanite + quartz = 3 $anorthite_{Pl}$

These reactions were calculated using the thermodynamic data set of Berman (1988) with activity models of Berman (1990), McMullin *et al.* (1991), Chatterjee and Froese (1975) and Fuhrman and Lindsley (1988). Reaction 3 was also calculated according to the calibration of Holdaway *et al.* (1988), reaction 4 also according to Newton & Haselton (1981) and Koziol and Newton (1988). Using temperatures calculated with the above methods, uniform pressures were calculated at 4 ± 0.2 kbar (4 samples). These calculated temperatures and pressures are slightly above the anatexis minimum curve and the muscovite+quartz outcurve for a_{H2O}=1.0 (Fig. 9). The paragenesis muscovite-sillimanite-K-feldspar-quartz is unusually widespread in central Bushmanland. Most fabrics point to a retrograde formation of muscovite. K/K+Na ratios of muscovite in coexistence with quartz, sillimanite and K-feldspar (0.95±0.02 for 22 samples) indicate formation about 5-10°C below their maximal thermal stability according to the experiments and calculations of Chatterjee and Flux (1986).

In two samples containing additional potassic feldspar, the following water-dependent multivariant reactions

(1) $Muscovite_{Ms}$ + $phlogopite_{Bi}$ + 3 quartz = 2 $orthoclase_{Kfs}$ + $pyrope_{Grt}$ + 2 H_2O
(2) 3 $Anorthite_{Pl}$ + 3 quartz + 2 $phlogopite_{Bt}$ = $orthoclase_{Kfs}$ + $grossular_{Grt}$ + 2 $pyrope_{Grt}$ + 2 H_2O
(3) $Muscovite_{Ms}$ + quartz = $orthoclase_{Kfs}$ + sillimanite + H_2O

cross near the determined PT-range, when calculated

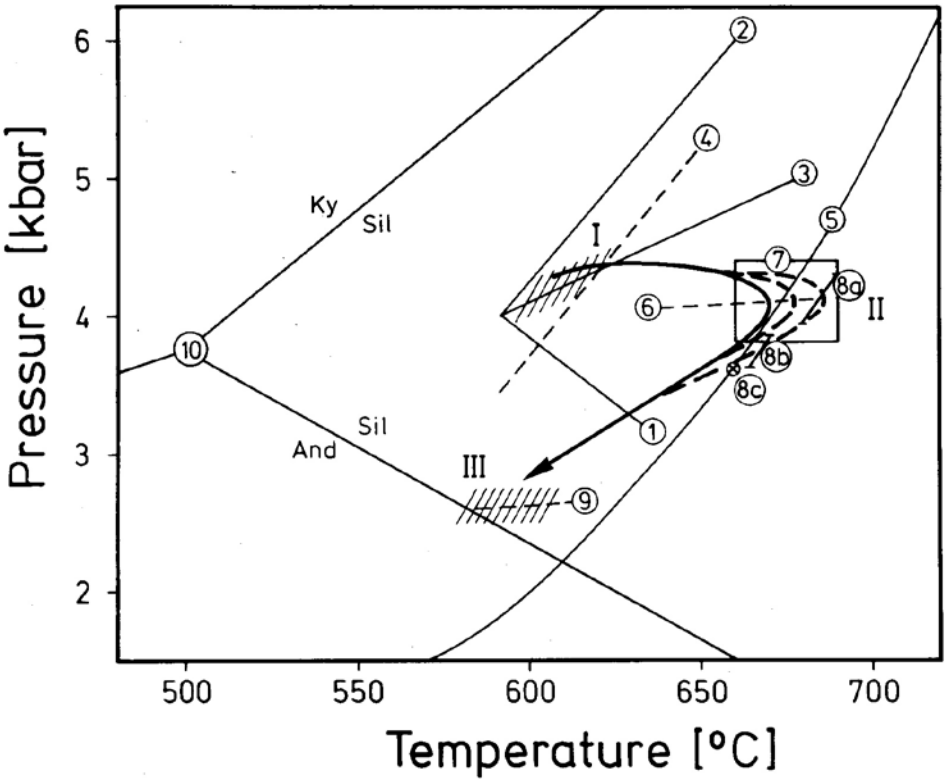

Figure 9: PT-diagram for the partial PT-path near the thermal maximum: 1 - X_{Fe}=0.6 for biotite in paragenesis with Crd-Sil-Qtz-Ms (Harte and Hudson 1979); 2 - X_{Fe}=0.6 for biotite in paragenesis with St-Sil-Qtz-Ms (Harte and Hudson, 1979); 3 - X_{Fe}=0.6 for biotite in paragenesis with Grt-Sil-Qtz-Ms (Spear and Selverstone, 1983); 4 - St + Crn = Hc + Sil calculated for sample 13634 (Willner, 1993); 5 - Ms + Qtz = Kfs + AS + V (Chatterjee and Johannes, 1974; a_{H2O} = 1.0); 6 - X_{Fe}=0.9 for garnet in paragenesis with Grt-Sil-Qtz-Ms (Spear and Selverstone 1983); 7 - maximal PT-conditions in central Bushmanland (see text); 8 - calculated maximal PT-data for the paragenesis Qtz-Pl-Bt-Grt-Sil-Kfs-H_2O at a_{H2O}=1.0; a- sample Sa 267; b- sample Sa 136; c- intersect of isopleth Si 3.06 p.f.u. of muscovites; 9 - X_{Fe}=0.95 for garnet rims in paragenesis with Bt-Qtz-Sil-Ms (Spear and Selverstone, 1983); aluminosilicate stability fields according to Holdaway (1971).

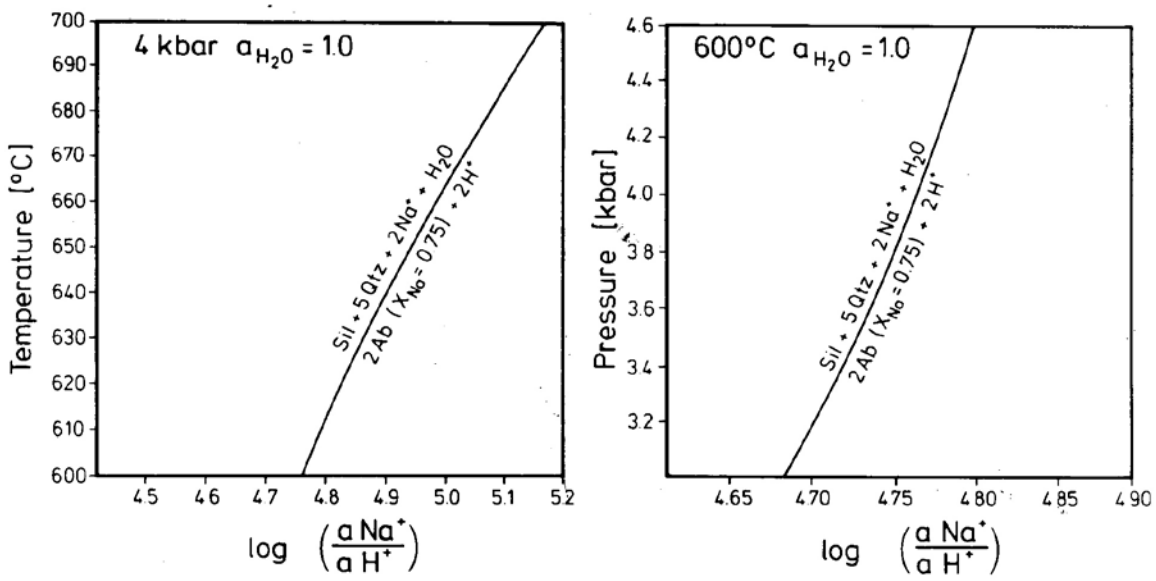

Figure 10: T/log (a_{Na+}/a_{H+}) and P/log (a_{Na+}/a_{H+})-diagrams with cation solution reactions for albite; calculated with Ge0-calc of Brown *et al.* (1988).

with the thermodynamic data set of Berman (1988) and assuming a water activity of 1.0 (Fig. 9).

This indicates retrograde formation of muscovite immediately passing peak temperature conditions. External water influx should have derived from water temporarily stored within partial melts which formed at water saturated conditions generally prevailing within the entire area.

Independently the same maximum pressures were calculated in two calc silicate rocks with the following water independent multivariant reaction using the thermodynamic data set of Berman (1988):

3 $Anorthite_{Pl}$ + 3 $diopside_{Cpx}$ = 3 quartz + $pyrope_{Ort}$ + 2 $grossular_{Ort}$

et al. (1988).

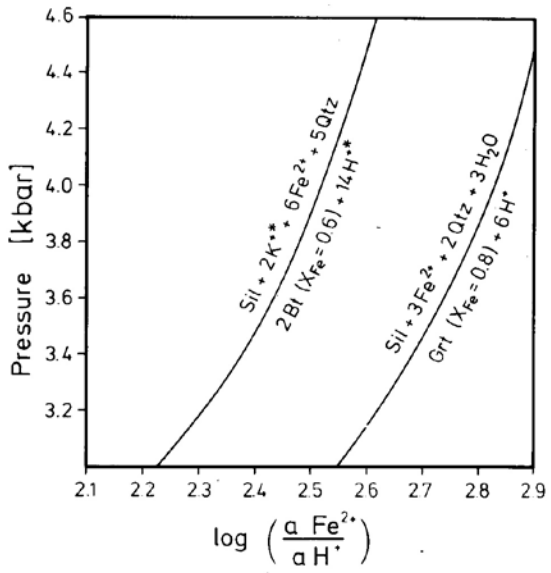

Figure 11: T/log (a_{Fe2+}/a_{H+}) and P/log (a_{Fe2+}/a_{H+})-diagrams with cation solution reactions for garnet and biotite (* a_{K+}/a_{H+} = 4); calculated with Ge0-calc of Brown *et al.*

Retrograde PT -data

The early retrograde PT-path is documented by increasing X_{Fe} at the garnet rims. In paragenesis with sillimanite-biotite-garnet-muscovite-quartz this indicates a definite pressure decrease with lower temperatures. The X_{Fe}-isopleth for the Mn-free garnet rims indicates pressures of 2.5 kbar at temperatures between 550-600°C (Fig. 9).

Most rocks in central Bushmanland are affected by late retrograde alteration due to a pronounced influx of an external fluid phase. In the sillimanite rocks large diaspore crystals may form with pyrophyllite in contact. Kaolinite forms at the contact between both minerals. This indicates that the relatively small stability field of diaspore-pyrophyllite was transsected (Fig. 14), while sillimanite in other rocks is directly altered to diaspore and kaolinite, which is more typical for lower pressures. PT-conditions during alteration should have been near the invariant point in Fig. 14 which may be shifted to lower pressures with decreasing water activity. Pressures in a comparable range of 1.5 kbar are indicated by the orientation of the isochore of late secondary CO_2-inclusions and Si-isopleths of sericitic white mica in rocks containing the limiting assemblage with chlorite, potassic feldspar and quartz (Massonne, 1991).

Discussion of the PT -evolution and crustal dynamic implications

Data and observations indicate that the entire central Bushmanland underwent a PT-path with five equilibration stages (Fig. 15). An equilibrium stage is understood here as a period of time during PT-evolution with temporal stagnation under constant PT conditions

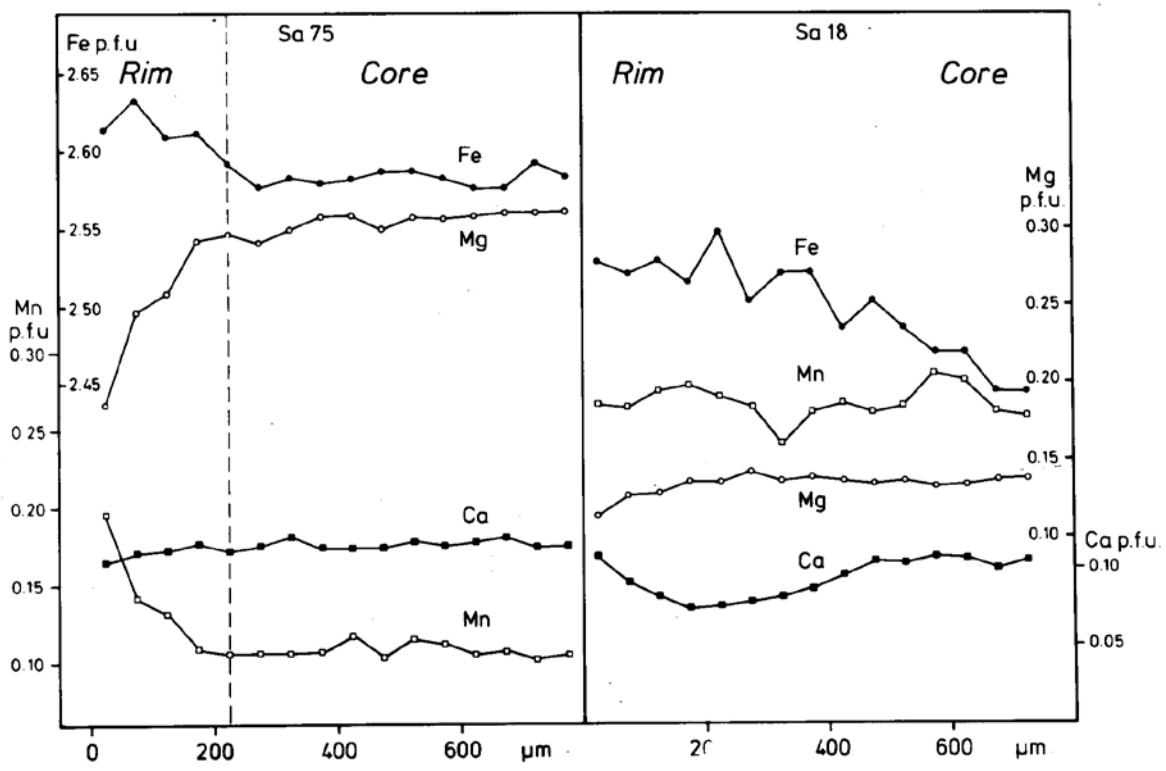

Figure 12: Quantitative garnet scans showing two types of zoning: Type A (sample Sa75) and type B (sample Sa18); (for explanation see text).

which was longer than the minimal time necessary for equilibration.

Rare pseudomorphs of topaz after andalusite indicate a possible prograde equilibration in the andalusite stability field (stage 1; Fig. 8). This may still be part of the late basin evolution, which is characterised by an elevated geotherm due to bimodal volcanism and pronounced exhalative deposits (Moore, 1986).

During the dominant deformation event D_2 a penetrative foliation was formed due to thrusting and crustal stacking (Joubert, 1974; Moore, 1977; Watkeys, 1986; Van Aswegen *et al.* 1987; Van der Merwe and Botha, 1989). Fibrolite is the only relic phase that may still be orientated parallel to the D_2-stretching lineation in many pelites and fibrolite-quartz-nodules in thrust horizons (Watkeys, 1986). Prismatic sillimanite always recrystallised in unorientated fashion across fibrolite.

This indicates that D_2-compression was synchronous

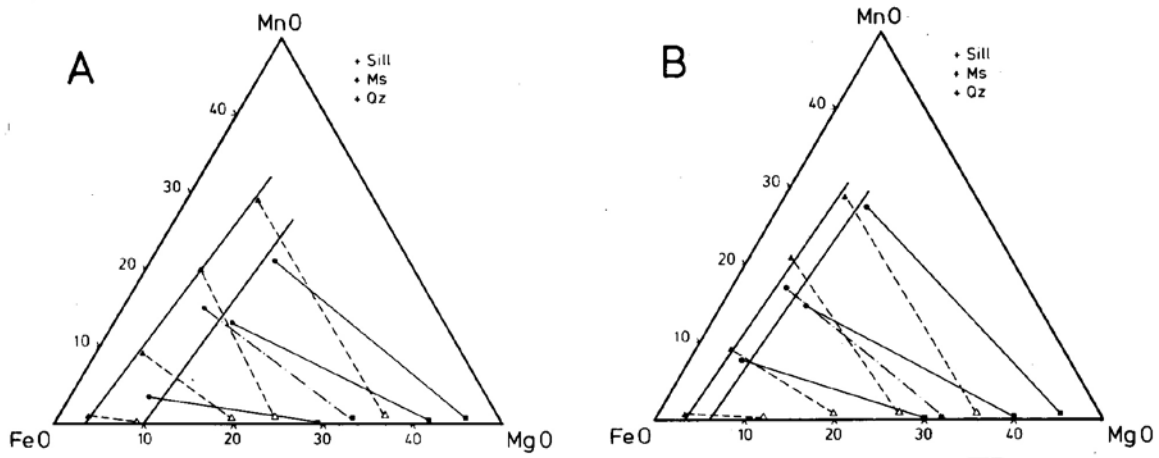

Figure 13: MnO-FeO-MgO projection for coexisting biotite and garnet in paragenesis with sillimanite, muscovite and quartz after Spear (1986). **I** - Garnet cores and matrix biotites; **II** - Garnet rims with biotites in contact. Two groups of coexisting biotite-garnet pairs are distinguished (see text): Group A with ruled tie lines (garnet A, biotite A); group B with ruled tie lines (garnet B, biotite B); explanation see text.

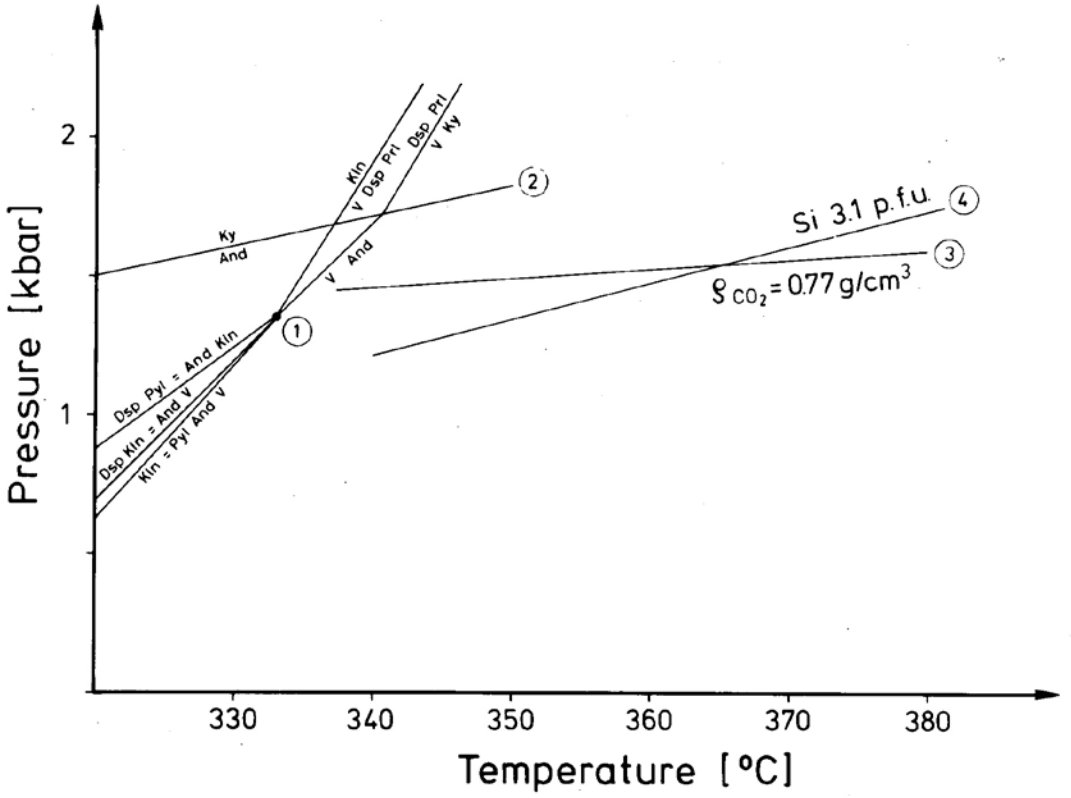

Figure 14: Retrograde PT data (see text); 1 - reactions involving diaspore, kaolinite, pyrophyllite, andalusite, kyanite and H_2O according to Chatterjee *et al.* (1984); 2 - Holdaway (1971); 3 - CO_2 isochore after Angus *et al.* (1976); 4 - Si isopleth for white mica in paragenesis with biotite, K-feldspar and quartz after Massonne (1991).

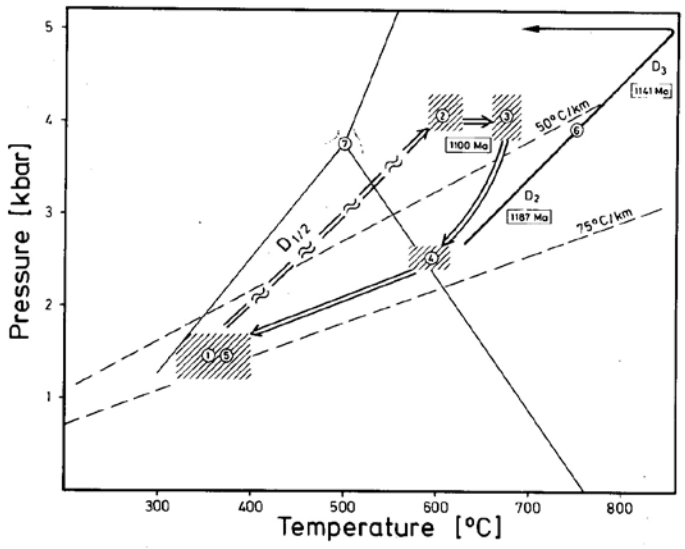

Figure 15: Synoptic PT-path for central Bushmanland; 1-5 stages of equilibration (see text); 6 - PT path for granulites of the southern Namaqua Mobile Belt (Waters, 1988); 7 - Aluminosilicate stability field after Holdaway (1971).

with prograde LP-HT metamorphism. This is an unusual time relationship that, however, may be observed in some other Proterozoic mobile belts e.g. in Australia (Loosveld, 1989; Reinhardt, 1992).

D_2-deformation stopped with equilibration at the pressure maximum of 4 kbar at 600°C before the thermal peak of metamorphism was reached. This stage 2 is derived from inclusion phases within pelites and peraluminous rocks. There is no indication that higher pressures were ever reached, which proves that only relatively thin crust was stacked. Analogous observations were made in higher grade areas to the south of the Bushmanland subprovince (Waters, 1990). Widespread fibrolitisation phenomena also indicate temperature and pressure increase during constant single pass fluid flow.

During thrusting and crustal stacking large volumes of multiple, sheet-like intrusions of strongly crustal contaminated I-type granites were emplaced and later deformed by D_2 (Watkeys, 1986; Duncan *et al.*, 1985). Hence the strongly elevated geotherm during thrusting may be due to basic magmatic accretion in the lower crust (Waters, 1990, 1991) and advective heat transport by large volumes of acid magmas within the crust (e.g. De Yoreo *et al.*, 1989). Already warm crust should have been stacked due to the retardation of heating with respect to the deformation event. Thus heating preceded and continued during convergence and lowered the viscosity of the crust.

Major equilibration at 680°C/4 kbar (stage 3) is well documented. Hence isobaric heating characterises the late prograde PT-path. Because post-kinematic granitoids are extremely rare in central Bushmanland, a mechanism other than magmatic heat supply may be envisaged.

In contrast to the observations made in central Bushmanland, the end of crustal stacking coincides with the thermal peak in the granulite areas of the southern Bushmanland subprovince (Fig. 15; Waters, 1988) at 750-860°C/5 kbar and isobaric cooling follows. Because HT/LP metamorphism is progressive in the entire Bushmanland subprovince without "P or T jumps" and D_2 deformation is considered comparable in the whole subprovince, there should be a link between both contrasting isobaric cooling paths. An explanation could be a thermal relaxation towards a joint high geotherm of about 45-50°C/km by conductive heating after crustal stacking, if a crustal slab with an originally lower geotherm is thrust over a slab with an originally higher geotherm within midcrustal levels (Fig. 16).

The early retrograde PT-path implies uplift corresponding to a decompression of about 1.5 kbar during cooling of ca. 100°C. Yet it must be borne in mind that this stage 4 is only defined by a "closing temperature" for diffusion processes in garnet. However, direction of the PT-path is well documented. Late retrograde mineral growth (stage 5) occurred due to a penetrative fluid infiltration at temperatures between 300 and 400°C/1.5

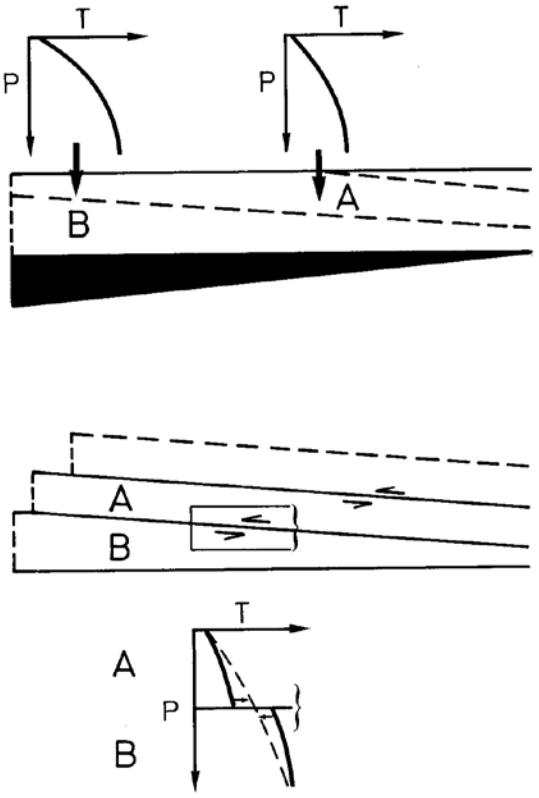

Figure 16: Model for the thermal evolution of the crust in the Bushmanland Subprovince of the Namaqua Mobile Belt before and after crustal stacking D_2. A - central Bushmanland (amphibolite facies); B - Namaqualand (low pressure granulites); basic magmatic underplating is schematically indicated in black.

kbar. This should have been a near-surface crustal level characterised by hydrothermal convection during an elevated geotherm (Wood and Walther, 1986). The entire retrograde PT-path indicates a further increase in the geotherm. This should be due to crustal extension. However, as yet, direct evidence for extensional deformation on the retrograde PT-path has not been recorded in the area, but might be confined to local retrograde shear belts.

The recorded clockwise PT-loop is inconsistent with thermal relaxation and uplift after continent-continent collision without external heat supply. In such a situation convergence occurs under lower geotherms and the sillimanite field is generally transected only during late decom-pression (Thompson and Ridley, 1987). However, crustal wide convergence unrelated to continent-continent collision is known from the Cenozoic central Andes affecting a convergent plate margin over 800 km in width including a 200-km-wide magmatic arc (Isacks, 1988). Here, current models postulate orthogonal convergence and stacking of a previously thinned crust heated and thus weakened due to magmatic accretion over a very flat subducting slab (Isacks, 1988). Longlasting evolution of an active convergent plate margin was in fact already assumed for the entire

Namaqua Mobile Belt (De Beer *et al.*, 1982; Hartnady *et al.*, 1985; Waters, 1991). Thus electrical and magnetic anomalies in the southern Cape ("Southern Cape Conductive Belt") are seen as indirect evidence of fossil oceanic crust being subducted toward the NE (De Beer and Meyer, 1983; De Beer *et al.*, 1982). Similar to the magmatic arc of the Cenozoic central Andes, the wide HT/LP-zone of the Bushmanland subprovince with calcalkaline magmatism lay some hundred km within the continent relative to the active Mesoproterozoic continental margin in southernmost Africa. Temporarily extremely flat orthogonal subduction is thought to have caused major crustal stacking of a previously heated and weakened continental crust.

Acknowledgements

The research leading to this publication was funded by the Deutsche Forschungsgemeinschaft DFG (Grants Wi 875/1,2). J. McStay and D. Strydom are thanked for their constructive reviews.

References

Angus, S., Armstrong, B., de Reuck, K.M., Altunin, V.V., Gadetskii, O.G., Chapela, G.A. & Rowlinson, J.S. 1976. International thermodynamic tables of the fluid state, **3**, Carbon dioxide. Pergamon, Oxford, 385pp.

Armstrong, R.A., Reid, D.L., Watkeys, M.K., Lipson, R.D., Welke, H.J. and Compston, W. 1988. Zircon U-Pb ages from the Aggeneys area, Central Bushmanland. *Ext. Abstr. Geocongr. 1988 Durban*, 493-499.

Berman, R.G. 1988. Internally-consistent thermodynamic data for minerals in the system Na_2O-K_2O-CaO-MgO-FeO-Fe_2O_3-Al_2O_3-SiO_2-TiO_2-H_2O-CO_2. *J. Petrol*., **29**, 445-522.

Berman, R.G. 1990. Mixing properties of Ca-Mg-Fe-Mn garnets. *Am. Mineral*., **75**, 328-344.

Blignault, H.J., Van Aswegen, G., Van der Merwe, S.W. and Colliston, W.P. 1983. The Namaqua Geotraverse and Environs: Part of the Proterozoic Namaqua Mobile Belt. *In*: Botha, B.J.V. (Ed.), *Namaqualand Metamorphic Complex*. Geol. Soc. S. Afr. Spec. Publ., **10**, 1-29.

Brown, T.H., Berman, R.G. and Perkins, E.H. 1988. GeO-Calc: Software package for calculation and display of pressure-temperature-composition phase diagrams using an IBM or compatible Personal Computer. *Comput. & Geosci.*, **14**, 279-289.

Chatterjee, N.D. and Johannes, W. 1974. Thermal stability and standard thermodynamic properties of synthetic 2M1-muscovite, $KAl_2[AlSi_3O_{10}(OH)_2]$. *Contrib. Mineral. Petrol*., **48**, 89-114.

Chatterjee, N.D. and Froese, F. 1975. A thermodynamic study of the pseudobinary join muscovite-paragonite in the system $KAlSi_3O_8$-$NaAlSi_3O_8$-Al_2O_3-SiO_2-H_2O. *Am. Mineral*., **60**, 985-993.

Chatterjee, N.D. 1976. Margarite stability and compatibility relations in the system CaO-Al_2O_3-SiO_2-H_2O as a pressure-temperature indicator. *Am. Mineral*., **61**, 699-709.

Chatterjee, N.D., Johannes, W. and Leistner, H. 1984. The system CaO-Al_2O_3-SiO_2-H_2O: new phase equilibria data, some calculated phase relations, and their petrological applications. *Contrib. Mineral. Petrol.*, **88**, 1-13.

Chatterjee, N.D. and Flux, S. 1986. Thermodynamic mixing properties of muscovite-paragonite crystalline solutions at high temperatures and pressures, and their geological applications. *J. Petrol*., **47**, 677-693.

Colliston, W.P., Praekelt, H.E., Strydom, D. and Loock, J.C. 1986. Aspects of the stratigraphy and depositional environment of part of the Bushmanland Group in the Aggeneys Terrane, Namaqua Mobile Belt. *Ext. Abstr. Geocongr. Johannesburg 1986*, 773-776.

Colliston, W.P., Praekelt, H.E. and Schoch, A.E. 1991. A progressive ductile shear model for the Proterozoic Aggeneys Terrane, Namaqua mobile belt, South Africa. *Precambr. Res.*, **49**, 205-215.

De Beer, J.H. and Meyer, R. 1983. Geoelectrical and gravitational characteristics of the Namaqua mobile belt and its boundaries. *Geol. Soc. S. Afr. Spec. Publ*., **10**, 91-100.

De Beer, J.H., Van Zijl, J.S.V. and Gough, D.I. 1982. The southern Cape Conductive Belt (South Africa): Its composition, origin and tectonic significance. *Tectonophysics*, **83**, 205-225.

De Yoreo, J.J., Lux, DR, Decker, E.R. and Osberg, P.H. 1989. The Acadian thermal history of western Maine. *J. metamorph. Geol*., **7**, 169-190.

Duncan, A.R, Joubert, P., Reid, A.M., Watkeys, M.K., Betton, P.J., Reid, D.L., Erlank, A.J. and Cleverly, R.W. 1985. *Geochemical studies on the floor rocks of Namaqualand*. NGP Final Report Univ. Cape Town (unpubl).

Ellis, D.J. and Green, D.H. 1979. An experimental study of the effect of Ca upon garnet-clinopyroxene Fe-Mg exchange equilibria. Contrib. *Mineral. Petrol*., **71**, 13-22.

Frick, C. and Coetzee, C.B. 1974. The mineralogy and the petrology of the sillimanite deposits west of Pofadder, Namaqualand. *Trans. Geol. Soc. S. Afr.*, **77**, 169-183.

Fuhrman, M.L. and Lindsley, D.H. 1988. Ternary feldspar modeling and thermometry. *Am. Mineral*., **73**, 201-215.

Ganguly, J. and Saxena, S.K. 1984. Mixing properties of aluminosilicate garnets: constraints from natural and experimental data, and applications to geothermobarometry. *Am. Mineral*., **69**, 88-97.

Guidotti, C.V. 1984. Micas in metamorphic rocks. *In*: Bailey, S.W. (Ed.): *Micas*. Rev. Mineral., **13**, 357-

467 (Mineralogical Society of America).

Harley, S.L. 1989. The origin of granulites: a metamorphic perspective. *Geol. Mag*., **126**, 215-247.

Harte, B. and Hudson, N.F.C. 1979. Pelite facies series and the temperatures and pressures of Dalradian metamorphism in E Scotland. *In*: Harris, A.L., Holland, C.H. and Leake, B.E. (Eds). *The Caledonides of the British Isles-reviewed*. Geol. Soc., London, Spec. Publ., **8**, 323-337.

Hartnady, C.J.H., Joubert, P. and Stowe, C.W. 1985. Proterozoic crustal evolution in Southwestern Africa. *Episodes*, **8**, 236-244.

Helgeson, H.C., Kirkham, D.H. and Flowers, G.C. 1981. Theoretical prediction of the thermodynamic behaviour of aqueous electrolytes at high pressures and temperatures: IV. Calculations of activity coefficients, osmotic coefficients, and apparent molal and standard and relative partial molal properties to 600C and 5 kb. *Am. J. Sci.*, **281**, 1249-1516.

Holdaway, M.J. 1971. Stability of andalusite and the aluminium phase diagram. *Am. J. Sci*., **271**, 97-131.

Holdaway, M.J., Dutrow, B.L. and Store, P. 1986. A model for the crystal chemistry of staurolite. *Am. Mineral.*, **71**, 1142-1159.

Holdaway, M.J., Dutrow, B.L. and Hinton, RW. 1988. Devonian and Carboniferous metamorphism in west-central Maine: The muscovite-almandine geobarometer and the staurolite problem revisited. *Am. Mineral*., **73**, 20-47.

Isacks, B.L. 1988. Uplift of the Central Andean Plateau and Bending of the Bolivian Orocline. *J. Geophys. Res*., **93**, 3211-3231.

Johannes, W. 1984. Beginning of melting in the granite system Qz-Or-Ab-An-H_2O. *Contrib. Mineral. Petrol*., **86**, 264-273.

Joubert, P. 1974. The gneisses of Namaqualand and their deformation. *Trans. Geol. Soc. S. Afr*., **77**, 339-345.

Joubert, P. 1986. Namaqualand - A model of proterozoic accretion? *Trans. Geol. Soc. S. Afr*., **89**, 79-96.

Kerrick, D.M. 1990. The Al_2SiO_5 polymorphs. *Reviews in Mineralogy, Mineralogical Society of America*, **22**, 406pp.

Koziol, A.M. and Newton, R.C. 1988. Redetermination of the anorthite breakdown reaction and improvement of the plagioclase-garnet-Al_2SiO_5-quartz geobarometer. *Am. Mineral*., **73**, 216-223.

Kretz, R. 1983. Symbols for rock-forming minerals. *Am. Mineral*., **68**, 277-279.

Loosveld R.J.H. (1989): The synchronism of crustal thickening and high-T/low-P metamorphism in the Mt. Isa inlier. *Tectonophysics*, **165**, 173-218.

Massonne H.-I. 1991. *High-pressure, low-temperature metamorphism of pelitic and other protoliths based on experiments in the system K_2O-MgO-Al_2O_3-SiO_2-H_2O*. Habilitation thesis, Univ. Bochum/Germany, 172 pp. (unpubl.).

McMullin, D.W., Berman, R.G. and Greenwood, R.J. 1991. Calibration of the SGAM thermometer for pelitic rocks using data from phase equilibrium experiments and natural assemblages. *Can. Mineral.*, **29**, 889-908.

Moore, J.M. 1977. The geology ofNamiesberg, Northern Cape. *Bull. Precambr. Res. Unit, Univ. Cape Town*, **20**, 69pp.

Moore, J.M. 1986. *A comparative study of metamorphosed supracrustal rocks from the western N amaqualand Metamorphic Complex*. PhD thesis, Univ. Cape Town, 376 pp. (unpubl.).

Newton, R.C., Charlu, T.V. and Kleppa, O.J. 1980. Thermochemistry of the high structural state plagioclases. *Geochim. cosmochim. Acta*, **44**, 933-941.

Newton, R.C. and Haselton, H.T. 1981. Thermodynamics of the garnet-plagioclase-Al_2SiO_5-quartz geobarometer. *In*: Newton R.C., Navrotsky A. and Wood B.J. (Eds), *Thermodynamics of minerals and melts*. Advances in physical geochemistry, **1**, 111-147, Springer, Berlin-New York.

Odling, N.E. 1988. Structural analysis and three-dimensional modelling at Gamsberg, N.W. Cape. *Bull. Precambr. Res. Unit, Univ. Cape Town*, **34**, 90 pp.

Perchuk, L.L. and Aranovich, L.Y. 1984. Improvement of the biotite-garnet geothermometer: correction for the fluorine content of biotite. *Dokl. Akad. Nauk SSSR*, **277**, 471-475.

Reid, D.L., Welke, H.J., Erlank, A.J. and Betton, P.J. 1987. Composition, age and tectonic settings of amphibolites in the Central Bushmanland Group, Western Namaqua Province, Southern Africa. *Precambr. Res*., **36**, 99-126.

Reid, D.L. and Welke H.J. 1988. Radiogenic and Stable isotope characteristics of the Aggeneys-Gams ore deposits, Central Bushmanland. *Ext. Abstr. Geocongr. 1988 Durban*, 497 -499.

Reinhardt, J. 1992. Low-pressure, high-temperature metamorphism in a compressional tectonic setting: Mary Kathleen Fold Belt, northeastern Australia. *Geol. Mag.*, **129**, 41-57.

Schreyer, W. 1987. Pre- or synmetamorphic metasomatism in peraluminous metamorphic rocks? *In*: Helgeson, G.C. (Ed.), *Chemical transport in metasomatic processes*. NATO ASI Series C, **218**, 265-296 (Reidel).

Spear, F.S. and Selverstone, J. 1983. Quantitative PT paths from zoned minerals: theory and tectonic applications. *Contrib. Mineral. Petrol*., **83**, 348-357.

Spear, F.S. 1988. Thermodynamic projection and extrapolation of high-variance mineral assemblages. *Contrib. Mineral. Petrol*., **98**, 346-351.

Strydom, D. and Visser, J.N.J. 1986. Nappe structures in the highly deformed Proterozoic metasedimentary Aggeneys-type sequence of western Bushmanland, South Africa. *Precambr. Res.*, **33**, 171-187.

Thompson, A.B. and Ridley, J.R. 1987. Pressure-temperature-time (P-T-t) histories of orogenic belts. *Phil. Trans. R. Soc. Lond.*, **A321**, 27-45.

Tracy, R.J. 1982. Compositional zoning and inclusions in metamorphic minerals. In: Ferry, JM (Ed.): Characterisation of metamorphism through mineral equilibria. *Rev. Mineral*., **10**, 355-397 (Mineralogical Society of America).

Tracy, R.J., Robinson, P. and Thompson, A.B. 1976. Garnet composition and zoning in the determination of temperature and pressure metamorphism, central Massachusetts. *Am. Mineral.*, **61**, 762-775.

Van Aswegen, G., Strydom, D., Colliston, W.P., Praekelt, H.E., Schoch, A.E., Blignault, H.J., Botha B.J.V. and Van der Merwe, S.W. 1987. The structural-stratigraphic development of part of the Namaqua Metarnorphic Complex, South Africa.- An example of Proterozoic major thrust tectonics. *In*: Kröner A. (Ed.), *Proterozoic lithospheric evolution*. Am. Geophys. Union Geodyn. Ser, **17**, 207-216.

Van der Merwe, S.W. and Botha, B.J.V. 1989. The Groothoek Thrust Belt in western Namaqualand; an example of a mid-crustal structure. *S. Afr. J. Geol*., **92**, 155-166.

Waters, D.J. 1986. Metamorphic zonation and thermal history of pelitic gneisses from western Namaqualand, South Africa. *Trans. Geol. Soc. S. Afr.*, **89**, 97-102.

Waters, D.J. 1988. Metamorphic evidence for the heating and cooling path of Namaqua1and granulites. *In*: Daly, J.S., Cliff, R.A. and Yardley, B.W.D. (Eds), *Evolution of metamorphic belts*. Geol. Soc. Spec. Publ., **43**, 357-363.

Waters, D.J. 1990. Thermal history and tectonic setting of the Namaqualand granulites, Southern Africa: Clues to Proterozoic crustal development. *In*: Vielzeuf, D. and Vidal, Ph. (Eds), *Granulites and crustal evolution*. 243-256, Kluwer Academic Publishers.

Waters, D.J. 1991. Hercynite-quartz granulites: phase relations, and implications for crustal processes. *Eur. J. Mineral*., **3**, 367-386.

Watkeys, M.K. 1986. The Achab gneiss: a “floor” in Bushmanland or a flaw in Namaqualand? *Trans. Geol. Soc. S. Afr.*, **89**, 103-116.

Watkeys, M.K. 1988. A spectrum of thrust related structures in Bushmanland. *Ext. Abstr. Geocongr. 1988* Durban, 729-732.

Willner, A.P. 1993. Grundlagen zur Dynamik der mittleren Erdkruste - PT-Pfad, Fluidentwicklung und Fluorverteilung in einer Modellregion im Namaqua Mobile Belt (Südafrika). 191 pp, Ferdinand Enke Verlag Stuttgart.

Wood, B.J. and Walther, J.V. 1986. Fluid flow during metamorphism and its implications for fluid-rock ratios. *In*: Walther, J.V. and Wood, R.J. (Eds), *Fluid-rock interactions during metamorphism*. Adv. in phys. geochem., **5**, 89-108, Springer.